Desalination and Water Treatment
www.deswater.com

doi:10.5004/dwt.2019.23835

153 (2019) 367–379
June

Enhanced adsorption of tetracycline antibiotics from pharmaceutical wastewater on expanded graphite composites modified by metal oxide

Zhi Song, Yu-Long Ma*, Cong-Er Li

State Key Laboratory of High-efficiency Coal Utilization and Green Chemical Engineering, College of Chemistry and Chemical Engineering, Ningxia University, Yinchuan 750021, China, Tel. +86 951 2062859, Fax +86 951 2062859, email: yulongma796@sohu.com (Y.-L. Ma)

Received 19 September 2018; Accepted 21 January 2019

ABSTRACT

Tetracycline (TC), a major pollutant in water, has an adverse effect on ecosystem and human health. Thus, it is urgent to remove but still remains a challenging. In this work, a new adsorbent of MnO_2 decorated on sodium hypochlorite treated expanded graphite (MnO_2/TEG) was developed by an in situ hydrothermal method, which exhibited a highly removal rate of 99.2% to pharmaceutical wastewater treated by flocculation. The structure and morphology of the adsorbent was studied by detailed physical characterization. Meanwhile, the main influencing factors on the adsorption behavior such as pH value, concentration, temperature of the solution, adsorption time, metal oxide species and MnO_2 loading amount were also investigated in detail. It was found that the electrostatic adsorption between Mn^{4+} in MnO_2/TEG and dimethylamino groups in TC molecules played an important role during the adsorption process. These excellent properties proved that the novel composite could be applied to remove TC residues in pharmaceutical wastewater.

Keywords: Adsorption; Tetracycline residues; Removal efficiency; Composite materials

1. Introduction

Tetracycline (TC), one of the most common antibiotics in practical application, is a kind of polycyclic and tetrastyroxylamide compound with antimicrobial properties [1,2]. As a broad-spectrum antibiotic, TC is often used for the prevention and treatment of human and animal diseases. However, TC is excreted directly into water bodies via pharmaceutical and livestock wastewater and poorly adsorbed in soil that TC has been frequently detected in surface water, ground water and even in drinking water [3,4]. The persistence of antibiotics in ecosystems could influence the evolution of microbial structure, thereby threatening the ecological health. Moreover, the selection pressure originating from residual antibiotics on the environmental microbe could encourage the formation and spread of antibiotic-resistant bacteria and genes in a long term [5,6]. Through the circulation and accumulation of the food chain, residual TC can indirectly or directly threaten human health. However, removal of TC antibiotic from water bodies is difficult due to its changeful occurrence state, low biodegradability, and complexity of molecular structures [7]. Therefore, great attentions have been focused on the developing efficient technologies for TC removal [8].

At present, numerous approaches including catalytic degradation [9,10], advanced oxidation [11–13], photodegradation [14–17], adsorption process [18–20], membrane separation technology [21] have been used to remove TC in wastewater [22]. Compared to other technologies, adsorption has distinctive advantages of easy operation, low cost, high removal efficiency at very low concentration, and no toxicities generated from intermediates and byproducts [23]. Numerous studies have been conducted on the removal of TC by different adsorbents like activated carbon [24,25], biochar [26], MOFs [27], zeolite [28] and ion exchange resin [29]. However, these adsorbents suffer the problem of limited adsorption ability, high cost or poor water stability. Hence, developing an adsorbent with high adsorption capacity, low production cost, excellent water

*Corresponding author.

stability, and environment friendly for TC removal should be conducted and studied urgently [30].

Recently, a large number of studies had shown that the adsorption of TC by composite materials showed great potential. The composite material not only can exert the advantages of the carrier in the material, such as large specific surface area, good water stability and controllable surface function, but also exert enhanced adsorption function from the material supported on carrier [31–34]. In this way, the adsorbent can be designed and prepared in a targeted manner, which allows specific pollutants in the wastewater to be efficiently and specifically removed. In a recent study by Zandipak et al. [35], the synthesized Fe_3O_4 nanoparticles were coated by SiO_2 and were then modified with CTAB by using a simple sol-gel method with selective etching. Xiong et al. [7] studied the adsorption of TC antibiotics from aqueous solutions by a multi-walled carbon nanotube (MWCNT) loaded iron metal-organic framework (MIL-53(Fe)) composite. In the study of Zhang et al. [36], Fe_3O_4@graphene (Fe_3O_4@G) magnetic nanocomposite was prepared via in situ precipitation method for the removal of oxytetracycline (OTC) and tetracycline (TC) from aqueous solution. The results showed that the composite exhibited a higher adsorption rate of TC in aqueous solution. The above reports not only prove that composite materials have more advantages in the adsorption process, but also provide new ideas for future research. Meanwhile, the research on TC antibiotics in aqueous solution has been very mature. The next research should focus on how to effectively remove the TC in pharmaceutical wastewater.

Expanded graphite (EG) is an inorganic porous carbon based adsorbent with a low density (0.002–0.010 g cm^{-3}), which is usually prepared from well-crystallized natural flake graphite [37]. It is potentially an excellent inexpensive adsorbent due to high porosity, weak polarity, hydrophobic nature and high selective sorption capacity to large organic compounds [38]. Similarly, EG can also be an excellent carrier. Under certain pH conditions, the metal oxide can form a strong coordination with the dimethylamino group in TC to achieve the purpose of adsorbing TC [39]. However, the metal oxide particles are easy to agglomerate, so that it is difficult to exert the desired adsorption performance. EG, as an adsorbent, has a two-dimensional nanosheets structure, and the nanosheets are over-stacked, making it difficult to exert its own advantages in the adsorption process. Loading the metal oxide particles on the EG surface not only avoids excessive stacking between the nanosheets in the EG, but also enhances the adsorption of the material. Therefore, this idea is very worthy of expecting to remove TC from pharmaceutical wastewater.

2. Experimental

2.1. Materials

Tetracycline hydrochloride (AR, 98%) and pharmaceutical wastewater (pH = 5, the initial concentration (C_0) of TC was 200 mg L^{-1}) were provided by Qiyuan Pharmaceutical CO., LTD, China. The main parameters of pharmaceutical wastewater were listed in Table 1. NaOH (AR, 96%), HCl (AR, 36%), $KMnO_4$ (AR, 98%), $Zn(NO_3)_2{\cdot}6H_2O$ (AR, 98%), $Cu(NO_3)_2{\cdot}3H_2O$ (AR, 98%), $Mg(NO_3)_2{\cdot}6H_2O$ (AR, 98%), $Fe(NO_3)_3{\cdot}9H_2O$ (AR, 98%), polyaluminum chloride (AR, 98%) and polyferric sulfate (AR, 98%) were all purchased from TianJinGuangFu Technology Development CO., LTD in Tianjin, China. NaClO (AR, 14%) was purchased from Aladdin Industrial Corporation. Expanded graphite (EG) was purchased from QingDaoChenYang CO., LTD in Qingdao, China.

Table 1
Main components of pharmaceutical wastewater

Pharmaceutical wastewater	
Parameters	Contents
pH	5
COD	2067 mg L^{-1}
TOC	922 mg L^{-1}
Protein	0.88 mg L^{-1}
Oxalate	4.5 mg ml^{-1}
Amino nitrogen	1.35 mg L^{-1}
Reducing sugar	1.6 mg L^{-1}
Total sugar	3.2 mg L^{-1}
Tetracycline hydrochloride	200 mg L^{-1}
Pigment	Uncertain
Inorganic ion	Uncertain
Microorganism	Uncertain

2.2. Preparation of composite materials

Expanded graphite (1 g) was added to the beaker. Sodium hypochlorite (120 ml) was then added to the above beaker and ultrasonically dispersed for 1 h at room temperature. Subsequently, the mixture was vigorously stirred for 48 h under a water bath with 50ºC. The mixture was washed with deionized water until the effluent was colorless. The product was dried at 100ºC for 12 h. Finally, the sodium hypochlorite treated expanded graphite (TEG) was obtained. The TEG powder (3.5 g) was ultrasonically dispersed in deionized water (350 ml) for 5 h. Different amounts (0.88 g, 2.33 g and 4.74 g) of metal salt (i.e. $KMnO_4$, $Zn(NO_3)_2{\cdot}6H_2O$, $Cu(NO_3)_2{\cdot}3H_2O$, $Mg(NO_3)_2{\cdot}6H_2O$, $Fe(NO_3)_3{\cdot}9H_2O$) were added to the above mixture and stirred rapidly for 2 h. The mixture was transferred to a Teflon-lined stainless steel autoclave and reacted at 130°C for 15 h. The product was washed with deionized water until the water was colorless. Subsequently, the product was dried at 100ºC for 12 h. The resulting powder was then calcined at 400ºC for 5 h (heating rate was 2ºC min^{-1}). Finally, the metal oxide modified TEG was obtained. In this study, taking MnO_2 modified TEG as an example, 60% in 60% MnO_2/TEG refers to the metal oxide loading amount.

2.3. Characterization

Scanning electron microscopy (SEM, Hitachi S-4800) and transmission electron microscopy (TEM, FEI Tecnai G20) were used to characterize the particle size, morphology and microstructure of the material. The energy dispersive X-ray spectroscopy (SEM-EDX, Hitachi S-4800) analysis focused

on the elemental composition and distribution of the material. The adsorption mechanism was studied by X-ray photoelectron spectroscopy tests (XPS, kratos-ultra DLD). TG analysis (thermogravimetric analysis) was carried out on the calcined samples in air up to 1000°C using a French SETARAM SETSYS-1750 instrument with a heating rate of 10°C min^{-1}. Zeta potential measurements using a zeta analyzer (90 Plus Zeta, Brookhaven) were performed with different pH. HPLC (CTO-10ASVP) was used to determine the TC concentration.

2.4. Adsorption experiments

A certain concentration of TC solution was added to the conical bottle. The pH of the solution was adjusted by using HCl or NaOH solution with concentration of 0.1 mol L^{-1}. The composite material (50 mg) was added to the above solution (50 ml) for static adsorption test. At different temperatures, the conical flask continues to stir (120 rpm) for a certain period of time. The TC concentration in the solution was measured by HPLC at fixed time points.

2.4.1. Adsorption kinetics

Adsorption kinetics is an important adsorption parameter for adsorption performance of adsorbents. Adsorption kinetics mainly studies the relationship between adsorption rate and time during the whole adsorption process [40]. The adsorption kinetics were fitted by the following equations:

The pseudo-first-order model:

$$\ln(q_e - q_{ti}) = \ln(q_e) - k_1 t \quad (1)$$

The pseudo-second-order model:

$$t/q_{ti} = 1/(k_2 q_e^2) + t/q_e \quad (2)$$

where k_1 (min^{-1}) refers to the first-order rate constant; k_2 (mg g^{-1} min^{-1}) refers to the second-order rate constant. q_e refers to the equilibrium adsorption capacity. q_{ti} (mg g^{-1}) refers to the amount of TC adsorbed at time t (min).

2.4.2. Adsorption isotherm

The study of adsorption isotherms can not only be used to describe the relationship between the adsorbent and the adsorbate, but also to reveal the adsorption properties [41,42]. Adsorption data can be explained by Langmuir and Freundlich isotherm models:

Langmuir model:

$$q_e = q_{max} K_L C_e/(1+K_L C_e) \quad (3)$$

Freundlich model:

$$q_e = k_f C_e^{1/n} \quad (4)$$

The linear forms of these models:

$$1/q_e = 1/(q_{max} K_L) \times 1/C_e + 1/q_{max} \quad (5)$$

$$\lg(q_e) = \lg(k_f) + 1/n \times \lg(C_e) \quad (6)$$

where q_e (mg g^{-1}) refers to the equilibrium adsorption capacity. q_{max} (mg g^{-1}) refers to the the maximum adsorption capacity. K_L refers to the Langmuir adsorption equilibrium constant and C_e (mg L^{-1}) refers to the equilibrium solution concentration. k_f refers to Freundlich constant. $1/n$ refers to the adsorption intensity.

2.4.3. Adsorption thermodynamics

Thermodynamic equilibrium constant K for the adsorption was calculated from intercept determined by plotting $\ln(q_e/C_e)$ vs. q_e using the method of Khan and Singh. The standard free energy change ΔG was calculated using the equation:

$$\Delta G = -RT \ln K \quad (7)$$

where ΔG refers to the Gibbs energy change, R refers to the molar gas constant, T refers to the absolute temperature.

The enthalpy change ΔH and entropy change ΔS were calculated by according to the follow equation:

$$\ln K = \Delta H/(-RT) + \Delta S/R \quad (8)$$

2.5. Flocculation treatment

Flocculation treatment technology for pharmaceutical wastewater was provided by pharmaceutical companies. The flocculation process can efficiently remove impurities from the pharmaceutical wastewater while maintaining the stability of the TC concentration in the wastewater. The flocculation process greatly reduces the pressure of the subsequent adsorption process. Specific implementation details are as follows: The dosage of polyaluminum chloride (PAC) and polymeric ferric sulfate (PFS) was 0.175 g L^{-1}, respectively. The above two drugs were added to pharmaceutical wastewater and mixed. The rotation speed was 50 rpm. Both coagulation and settling time were 50 min. Subsequently, the above mixture was centrifuged (5000 rpm, 5 min), and the precipitate was removed. Finally, the pharmaceutical wastewater after flocculation treatment was obtained (pH = 5, C_0 = 180 mg L^{-1}).

3. Results and discussion

3.1. Characterization of composite material

The SEM images of different samples (graphite, EG, TEG, 20%MnO_2/TEG, 40%MnO_2/TEG and 60%MnO_2/TEG) are illustrated in Fig. 1. There were no big difference in the micromorphology of graphite, EG and TEG. It was found that the above three materials were stacked by flexible nanosheets with some wrinkles. As shown in Figs. 1d–f, petal-like MnO_2 nanoparticles appeared on the surface of the modified material, and the distribution of nanoparticles became more dense with the increase of loading amount. In order to further verify the difference between the samples, the morphology of the materials were characterized by TEM technology. As shown in Figs. 2a–c, consistent with the SEM characterization results, graphite, EG and TEG were composed of surface-wrapped nanosheets. When MnO_2

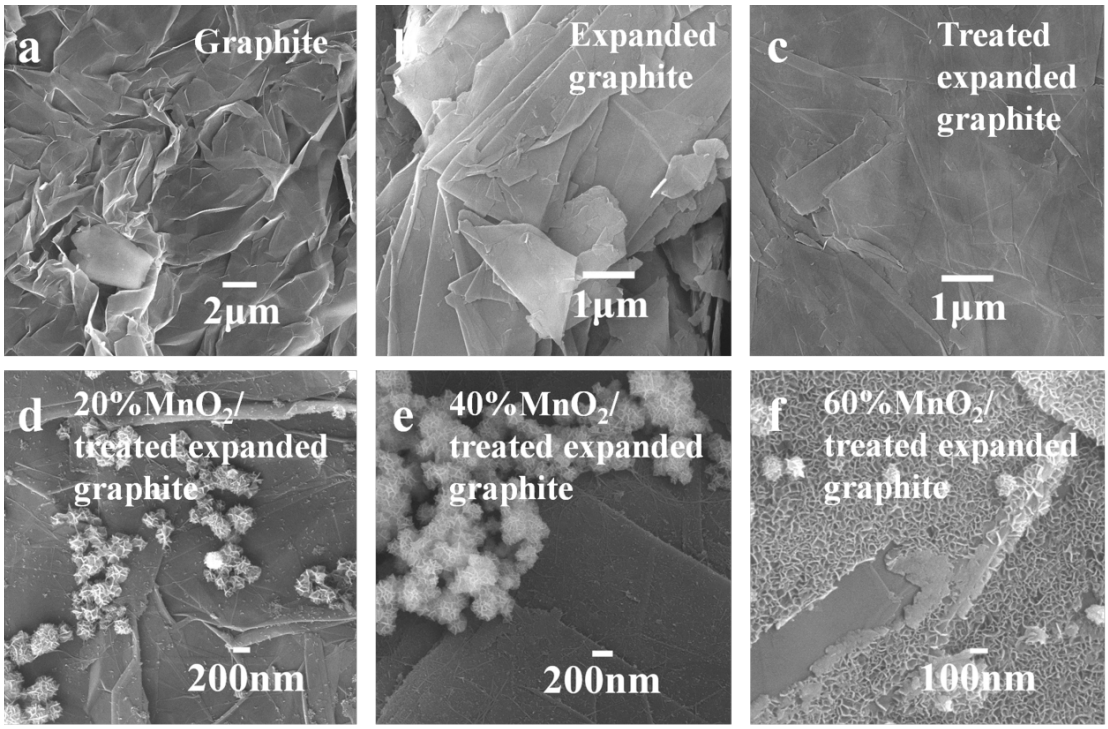

Fig. 1. SEM images of different samples.

was introduced onto the surface of the TEG, the petal-like nanoparticles were firmly loaded on both sides of the sheets to form a sandwich-like structure (MnO_2 nanoparticles/TEG/MnO_2 nanoparticles). This structure well avoided excessive stacking between the nanosheets, and then, there was more contact between the adsorbent and the adsorbate in the adsorption test, which enhanced the adsorption of composite materials. Moreover, with the increase of MnO_2 loading amount, the number of MnO_2 nanoparticles on TEG surface increased (Figs. 2d–f).

The elemental composition of MnO_2/TEG was characterized by EDX and EDX mapping (Figs. 3a–c and a1–c1, Figs. 3d–g), and EDX analysis indicated the presence of only C, O and Mn. The mapping results confirmed the presence and uniform distribution of C, O and Mn on the surface of 60%MnO_2/TEG. The elemental composition of TEG modified by different metal oxides was characterized by EDX, and the result is shown in Fig. 4.

As shown in Figs. 5a–c, compared with graphite, EG and TEG, there was no obvious change in the XPS spectra of the three materials. In other words, after treatment, the difference between the three materials was a slight increase in the O-C=O group. After the introduction of MnO_2, the type and amount of oxygen-containing functional groups of the composites increased significantly with the increase of the amount of potassium permanganate used during the modification (Figs. 5d–f). Taking 60%MnO_2/TEG as an example, the C1s peak included four peaks, at 284, 285, 288 and 291 eV, which were attributable to graphene, C-O, C=O, and O-C=O groups species, respectively. The introduction of a large number of oxygen-containing functional groups enhanced the interaction between the adsorbent and the adsorbate.

The temperature-mass relation was also studied (Fig. 6). All samples maintained good stability at the temperature below 400°C. There was two-stage process in the temperature-responsive mass evolution: the adsorbed/hydrated water went lost at temperatures, up to 200°C for graphite, EG and TEG, 345°C for 20%MnO_2/TEG, 355°C for 40%MnO_2/TEG and 430°C for 60%MnO_2/TEG; and then the rupture of chains, fragments and monolayers of graphite, EG and TEG. In addition, when the temperature was raised from 200 to 570°C, graphite, EG and TEG had different temperature-responsive mass evolution processes. Oxygen species were introduced into these three materials to form oxygen-containing functional groups, which made the quality of these three materials slightly increase. This result is consistent with the XPS characterization. After the introduction of MnO_2, the thermal stability of the composites (MnO_2/TEG) was greatly reduced due to the introduction of a large number of oxygen functional groups in the process of modification, which made the chains, fragments and monolayers of TEG more easily broken. Furthermore, the decomposition temperature of composites increased with the increase of MnO_2 loading amount.

3.2. Adsorption performance

3.2.1. Effects of different metal oxides

As shown in Fig. 7d, the effect of different metal oxides in the adsorption process was initially evaluated. The TC aqueous solution was used as the research object, and its initial concentration and pH were 200 mg L^{-1} and 4, respectively. The pH of the TC aqueous solution was adjusted to 5, which was consistent with the pH of the pharmaceuti-

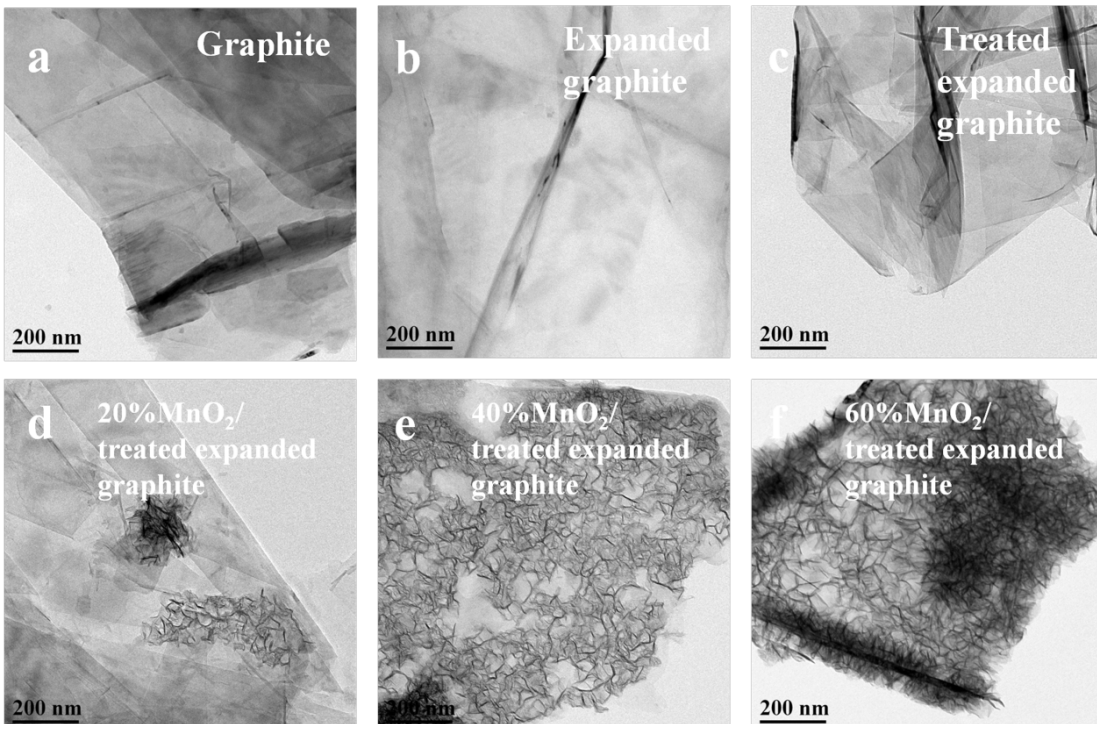

Fig. 2. TEM images of different samples.

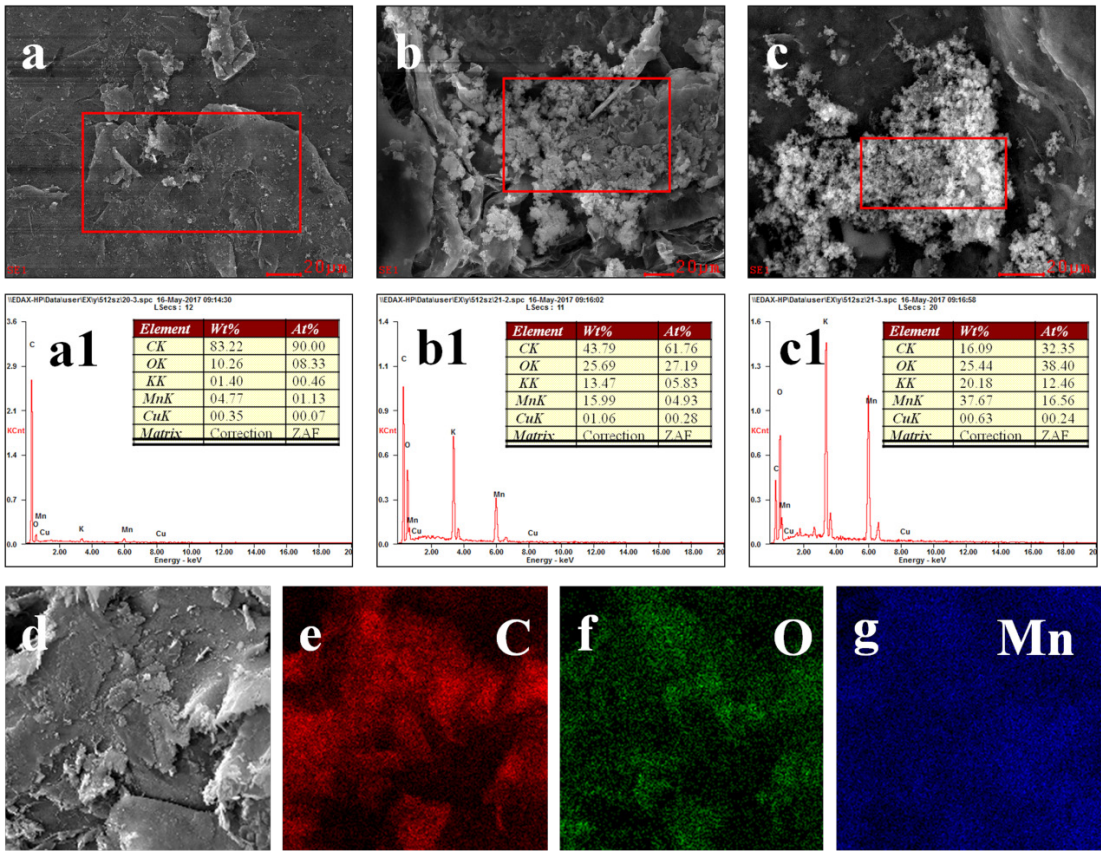

Fig. 3. (a) ~ (c) and (a1) ~ (c1) EDX spectrum of major elements on the MnO_2/TEG; (d) ~ (g) EDX mapping images of major elements on the 60%MnO_2/TEG.

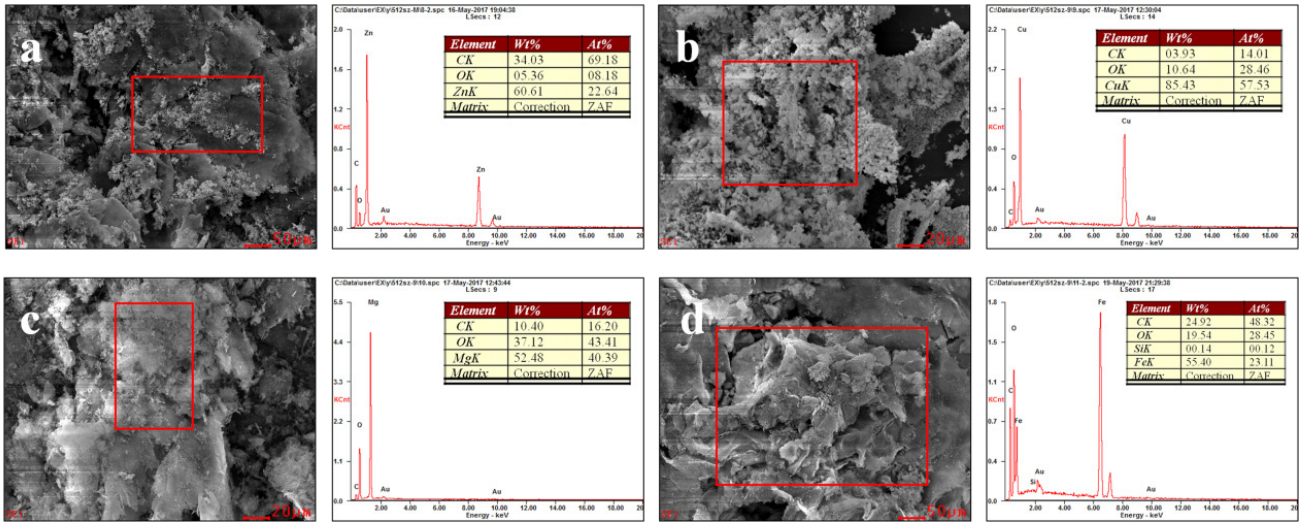

Fig. 4. EDX spectrum of major elements on the different samples ((a) 60%ZnO/TEG, (b) 60%CuO/TEG, (c) 60%MgO/TEG and (d) 60%Fe_2O_3/TEG).

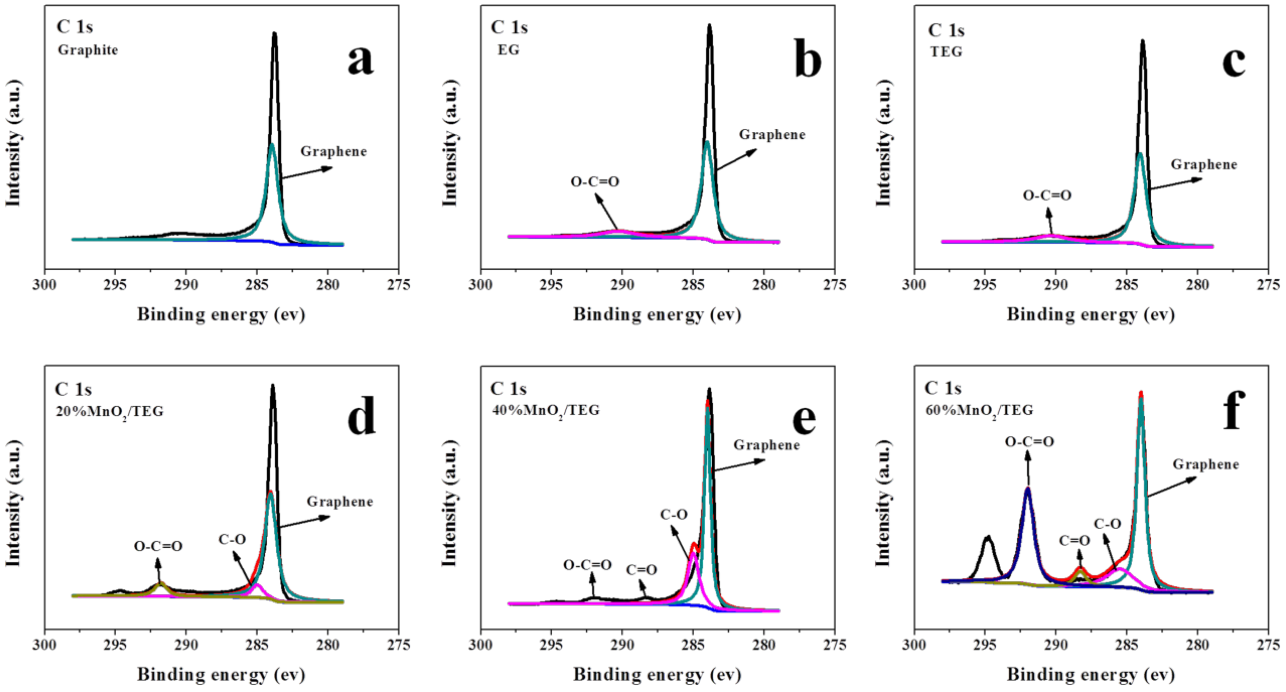

Fig. 5. C1s XPS spectra of different samples.

cal wastewater. The samples (60%ZnO/TEG, 60%CuO/TEG, 60%MgO/TEG, 60%Fe_2O_3/TEG and 60%MnO_2/TEG) were subjected to static adsorption testing using the static adsorption method described in section 2.4. After static adsorption for 21 h, the concentration of TC in solution was determined by HPLC. The results showed that TC removal rate by different adsorbents followed this trend: 60%MnO_2/TEG > 60%ZnO/TEG > 60%MgO/TEG > 60%CuO/TEG > 60%Fe_2O_3/TEG. Therefore, the subsequent experiments were based on 60%MnO_2/TEG.

3.2.2. *Effect of different MnO_2 loading amount*

After determining the type of metal oxide, it is necessary to further explore the effect of metal oxide loading amount on the adsorption results. A designed concentration of TC solution (pH = 5, 50 ml, C_0 = 200 mg L^{-1}) was added to the conical flask. Adsorbents (TEG with different MnO_2 loading amount, 50 mg) were added to the above solution for static adsorption (120 rpm, 21 h). As shown in Fig. 7f, compared with TEG, the adsorption rate of TC on MnO_2/TEG increased signifi-

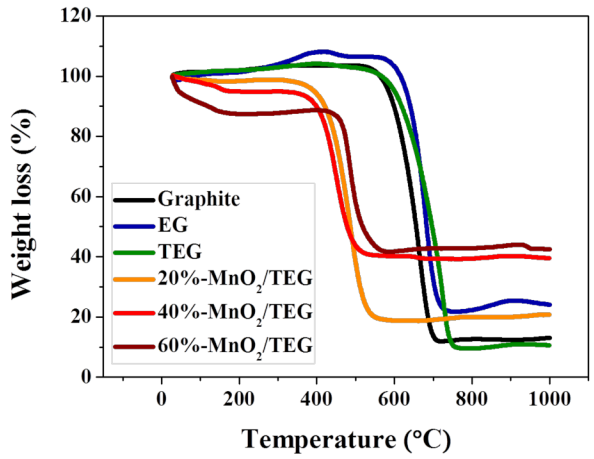

Fig. 6. TG curves of different samples.

cantly after the introduction of MnO_2. At the same time, TC adsorption rate increased with the increase of MnO_2 loading amount. However, considering the composite preparation cost and adsorption rate, the MnO_2 loading amount in this study was determined to be 60%.

3.2.3. Effects of adsorption time and solution pH

In order to facilitate to further study the adsorption mechanism, TC solution (C_0 = 200 mg L^{-1}, pH = 4) was selected as the research object in this study. The pH value of equivalent TC solution (50 ml) was adjusted to 3, 5, 7 and 9, respectively. Static adsorption tests of graphite, EG, TEG and 60%MnO_2/TEG were carried out using static adsorption method described in the section 2.4 (Figs. 7a–c, e). Solution pH is a key factor that could directly affect the TC adsorption rate by changing the adsorbent surface charge, the speciation distribution of the adsorbate and the ionization degree. The adsorption capacity of all adsorbents for TC increased with the increase of adsorption time. Except the 60%MnO_2/TEG, the adsorption capacity of adsorbents (graphite, EG and TEG) to TC increased with the increase of pH value. The TC adsorption capacity of graphite reached the highest (148 mg g^{-1}) when the pH value was 9. The TC adsorption capacity of EG and TEG reached the highest (170 mg g^{-1}, 152 mg g^{-1}) when the pH value was 7. However, the adsorption capacity of 60%MnO_2/TEG to TC decreased with the increase of pH value. At the pH of 3, the adsorption capacity of 60%MnO_2/TEG reached highest (198 mg g^{-1}); At the pH of 5, the adsorption capacity of 60%MnO_2/TEG was 193 mg g^{-1}. The adsorption capacity of 60%MnO_2/TEG at pH 5 was very close to that of pH 3. Meanwhile, the initial pH of pharmaceutical wastewater was 5. Therefore, in order to ensure that the adsorption test was closer to practical application, the optimal pH value and adsorption time in this study were 5 and 21 h, respectively.

3.2.4. Effect of solution concentration and temperature

At different test temperatures (298, 308 and 318 K), 60%MnO_2/TEG (50 mg) was added to TC solution (50 ml) with different concentrations (100, 200, 300, 400, 500, 700 and 1000 mg L^{-1}) for static adsorption test. The adsorption rate decreases with increase of TC solution concentration (Fig. 5c). But, with increase of test temperature, the TC adsorption rate showed an upward trend under the same solution concentration. Therefore, temperature is an important factor that can directly affect the TC adsorption rate.

3.2.5. Practical application in pharmaceutical wastewater

Based on the above research, the 60%MnO_2/TEG was put into practical application. TC adsorption rates in different solutions, such as, pharmaceutical wastewater (C_0 = 200 mg L^{-1}), pharmaceutical wastewater after flocculation treatment (C_0 = 180 mg L^{-1}) and TC solution (C_0 = 200 mg L^{-1}) were tested under the same conditions (pH = 5, adsorption time was 21 h). The static adsorption experiments of adsorbents in different solutions were carried out by using the method described in section 2.4. As shown in Fig. 7h, TC adsorption rate in pharmaceutical wastewater by 60%MnO_2/TEG was relatively low (53.9%). However, TC adsorption rates increased significantly in the other two solutions (99.2% and 99.4%). Pharmaceutical wastewater comes from pharmaceutical industry wastewater treatment systems. Therefore, its composition is very complicated, and it also contains a large amount of impurities, which has a great impact on the specific adsorption of TC. In practical applications, the use of flocculation technology to effectively remove impurities from pharmaceutical wastewater can reduce the pressure on subsequent adsorption processes.

3.3. Adsorption kinetics

The time profile for the adsorption of TC in aqueous solution by MnO_2/TEG with different MnO_2 loading amount is shown in Fig. 7f. Taking the adsorption of TC in aqueous solution by 60%MnO_2/TEG as an example, the adsorption equilibrium was reached at 1000 min. In other words, the adsorption rate of TC by 60%MnO_2/TEG increased rapidly within 200 min, and then the adsorption rate increased slowly until the adsorption equilibrium was reached. As shown in Table 2, the adsorption data can be better fitted to the pseudo-second-order kinetic model (R^2 = 0.9996). Furthermore, the adsorption capacity calculated $q_{e,cal}$ (195.3 mg L^{-1}) from pseudo-second-order equation was more consistent with the experimental $q_{e,exp}$ (195.8 mg L^{-1}) value. The above results indicate that the adsorption of TC by 60%MnO_2/TEG is a selective chemisorption. The adsorption mechanism will be discussed in detail in section 3.6.

3.4. Adsorption isotherm

The adsorption of TC in aqueous solution with different concentration by 60%MnO_2/TEG was studied at three different adsorption temperatures (Fig. 7g and Table 3). By comparing the correlation coefficients (R^2), Langmuir model is better to describe the TC adsorption isotherms on 60%MnO_2/TEG. Thus, monolayer adsorption dominated the adsorption process with contributions from heterogeneous adsorption [43]. At different temperatures, the maximum adsorption capacity values determined by Langmuir isotherm were 980, 980 and 1117 mg g^{-1}, respectively,

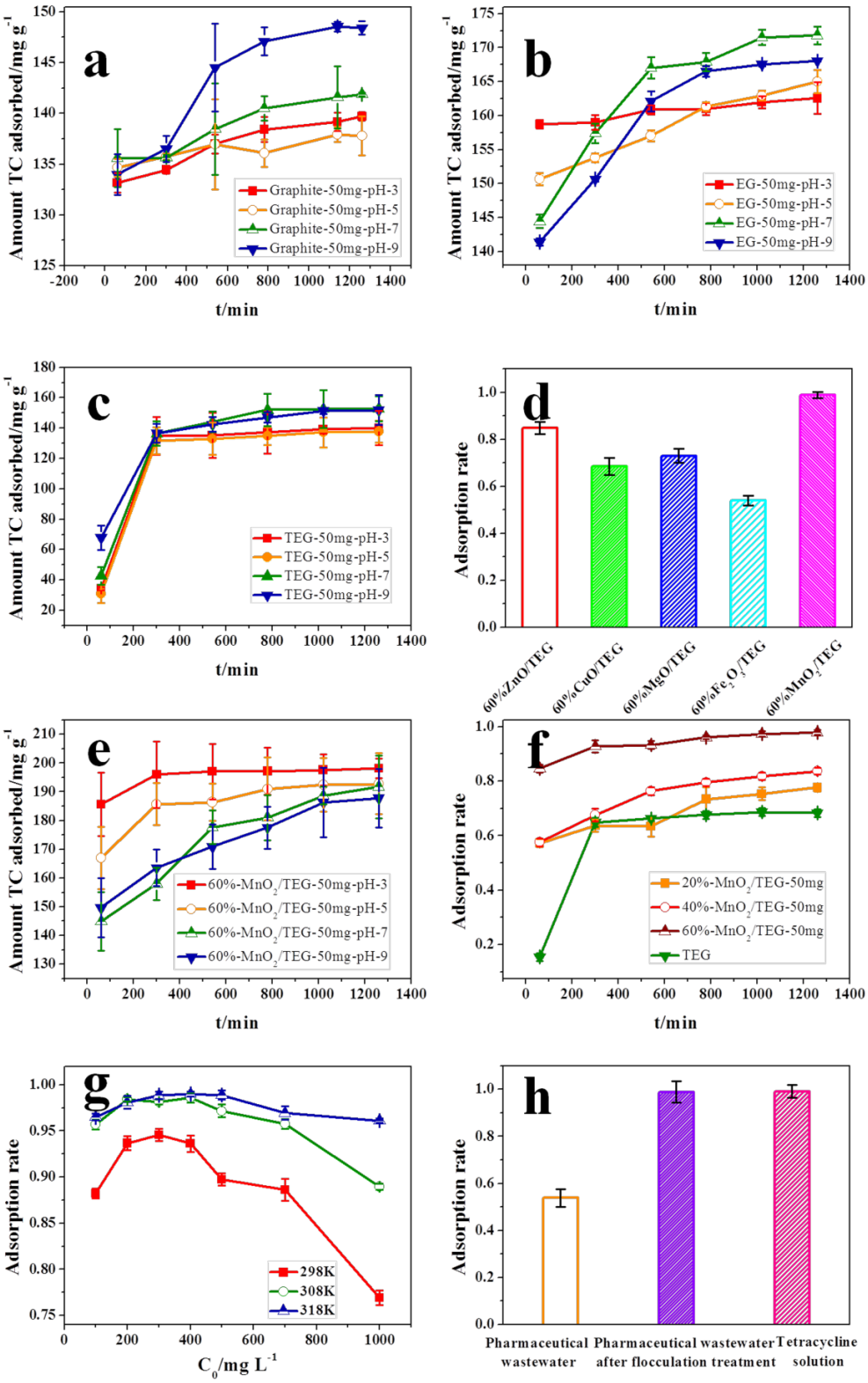

Fig. 7. (a) Adsorption capacity of graphite in TC aqueous solution with different contact time at different pH; (b) Adsorption capacity of EG in TC aqueous solution with different contact time at different pH; (c) Adsorption capacity of TEG in TC aqueous solution with different contact time at different pH; (d) Adsorption rate of TC by different metal oxide modified TEG; (e) Adsorption capacity of 60%MnO_2/TEG in TC aqueous solution with different contact time at different pH; (f) Adsorption capacity of MnO_2/TEG with different MnO_2 loading amount in TC aqueous solution (pH = 5); (g) Adsorption rate of TC in aqueous solution by 60%MnO_2/TEG at different temperatures with different concentrations; (h) Adsorption rate of 60%MnO_2/TEG in different solution.

Table 2
Adsorption kinetics fitted parameters

Samples	Pseudo-first-order		Pseudo-second-order		
	K_1 (min^{-1})	R^2	q_e ($mg\ g^{-1}$)	$K_2 \times 10^{-4}$ ($g\ mg^{-1}\ min^{-1}$)	R^2
Graphite	0.0012	0.6572	143.06	3.99	0.9982
Expanded graphite	0.0013	0.9653	169.49	2.64	0.9976
Treated expanded graphite	0.0019	0.9847	141.84	2.40	0.9996
60%MnO/TEG	0.0030	0.9046	195.31	3.13	0.9996

Table 3
Adsorption isotherms fitted parameters of 60%MnO_2/TEG

T (K)	Langmuir			Freundich		
	q_{max} ($mg\ g^{-1}$)	K_L ($L\ mg^{-1}$)	R^2	k_f	n	R^2
298	980	0.0188	0.8918	68.07	2.15	0.8249
308	980	0.0794	0.9413	151.89	2.49	0.8198
318	1117	0.1497	0.9767	188.53	2.14	0.7681

which indicated that higher initial concentration and higher adsorption temperature were conducive to adsorption. The K_L value from Langmuir model increased with the increase of temperature, indicating that the binding between TC and the active center of adsorbent increased with the increase of temperature, which also indicated that the adsorption process was endothermic [43].

3.5. Adsorption thermodynamics

The negative ΔG value indicated that the adsorption of 60%MnO_2/TEG to TC was a spontaneous adsorption process. The positive ΔH value indicated that the adsorption reaction had typical endothermic properties. The results showed that the adsorption capacity of TC increased with the increase of temperature, and the higher temperature promoted the adsorption of TC by 60%MnO_2/TEG (Figs. 7g and 8, Table 4).The positive ΔS value indicated an increase in the degree of randomness at the adsorbate-adsorbent interface. In solution, TC was surrounded by a tightly bound hydration layer where water molecules were more highly ordered than in the bulk water [30]. When the TC molecules came into close interaction with the hydration surface of 60%MnO_2/TEG, the ordered water molecules in these two hydration layers were compelled and disturbed, which would contribute to the increase of entropy [30]. Although the adsorption of TC molecules on 60%MnO_2/TEG surface caused the degree of freedom of TC molecules to decrease, it seemed likely that positive entropy related to the adsorption of TC on 60%MnO_2/TEG was due to the entropy increase of water molecules overweighing the entropy decrease of TC molecules [30].

Table 4
Calculated thermodynamic parameters of 60%MnO_2/TEG

T (K)	K	ΔG ($kJ\ mol^{-1}$)	ΔS ($J\ mol^{-1}\ K^{-1}$)	ΔH ($kJ\ mol^{-1}$)
298	38.58	–9.05	304.18	81.16
308	191.01	–13.45		
318	298.99	–15.07		

3.6. Adsorption mechanism

In this study, the interaction between adsorbent and adsorbate mainly has the following four types, such as, H-bonding, π-π interactions, electrostatic interaction and coordination effect (Table 5). It had been emphasized in section 3.2.3 that the solution pH is a key factor that could directly affect the adsorption rate. Solution pH not only directly affected the morphological distribution and ionization of the adsorbate, but also affected the change of the adsorbent surface charge. Under different acid dissociation constants (pKa = 3.3, 7.7, and 9.7), TC exists as a cationic (TCH_3^+), zwitter ionic (TCH_2^0), and anionic (TCH^- or TC^{2-}) species, respectively.

As shown in Fig. 7a, the adsorption capacity of equivalent graphite to TC in aqueous solution increased with the increase of pH. The adsorption capacity reached the highest when the solution pH was 9. At this pH, TC molecules existed as anionic (TCH^- or TC^{2-}) species. As shown in Fig. 10a, at pH of 9, the surface of the graphite was distributed with a strong negative charge. At this time, there was a strong electrostatic repulsion between the TC molecule and the adsorbent, which was very disadvantageous to the adsorption process. Graphite contained only a very small amount of oxygen-containing functional groups, indicating that there was almost no H-bonding interaction between graphite and TC molecules. Similarly, there were no metal oxides loaded on the surface of graphite. Therefore, the possibility that the metal oxide formed a coordination effect with N on the dimethylamino group in the TC molecule was also excluded. In addition, as shown in Table 2, the

Table 5
Adsorption performance parameters of adsorbents

Samples	Electrostatic interaction	H-bonding	Coordination effect	π-π interactions
Graphite	–	–	–	+
Expanded graphite	+	+	–	+
Treated expanded graphite	+	+	–	+
60%MnO/TEG	++	++	+	++

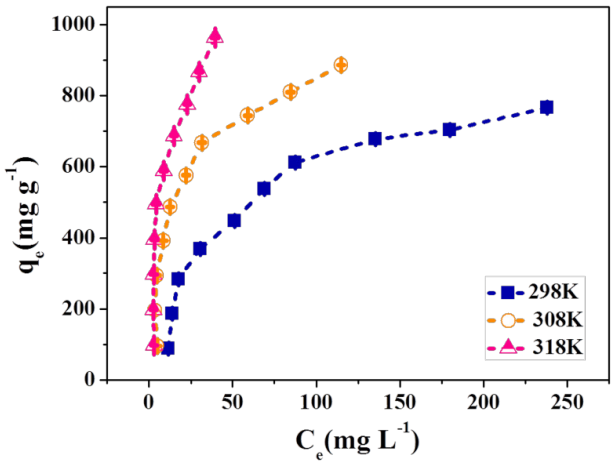

Fig. 8. Isotherm graph for TC adsorption.

adsorption of TC by graphite was selective chemisorption, and therefore, it was presumed that the interaction between graphite and TC was mainly π-π interaction.

As shown in Figs. 7b and c, the adsorption capacity of TC in aqueous solution by EG and TEG also increased with the increase of pH. At the pH of 7, the adsorption capacity reached their highest. The above two materials have very similar physicochemical properties, such as similar microscopic morphology (Figs. 1b, 1c, 2b and 2c), containing very small amounts of oxygen-containing functional groups (Figs. 5b and c), similar thermal stability (Fig. 6) and potential distribution (Figs. 10b and c), and approximate TC adsorption capacity (Figs. 7b and c). Among them, when the pH was 7, the two materials had strong negative electricity on the surface. At the same pH, TC molecules existed as zwitter ionic (TCH_2^0) species. Thus, there was a certain electrostatic interaction between the adsorbents and the TC molecules. Because of the presence of a certain amount of oxygen-containing functional groups in the adsorbents, it was possible for the adsorbents to form a certain amount of H-bonding interaction with the TC molecules.MnO_2 nanoparticles were not introduced in both EG and TEG, so there was no coordination between the adsorbents and TC molecules. In addition, TC molecules could interact with benzene ring structures on graphene sheets in the adsorbents to form π-π interactions. In summary, compared with graphite, EG and TEG had a higher TC adsorption rate.

As shown in Fig. 7e, the adsorption capacity of 60%MnO_2/TEG for TC in aqueous solution decreased with the increase of pH. At the pH of 3, the adsorption capacity reached the maximum. As shown in Fig. 10d, the surface of the adsorbent exhibited a strong negative charge at pH of 5. TC molecules existed as cationic (TCH_3^+) species under the same pH conditions. Therefore, a strong electrostatic attraction between the adsorbent and TC molecule could be generated, thus achieving the goal of TC adsorption. As shown in Fig. 5f, the adsorbent contains a large number of different oxygen-containing functional groups. Therefore, the C-OR groups on the surface of 60%MnO_2/TEG could form H-bonding with –OH groups on the TC molecule. As shown in Figs. 7c and f, the adsorption capacity of 60%MnO_2/TEG for TC was 198 mg g^{-1}, even higher than that of TEG (137 mg g^{-1}). The increase of adsorption capacity should be due to the MnO_2 nanoparticles, where nanoparticles avoided the over stacking of TEG sheets during adsorption. Therefore, TC molecules have more opportunities to interact with benzene ring structures on 60%MnO_2/TEG to form π-π interactions, which is advantageous to adsorption. In order to better explain the adsorption mechanism of TC on 60%MnO_2/TEG, XPS characterization was performed on samples before and after application. The XPS characterization results showed that the characteristic peak of the C-OR group appeared in the C1s spectrum of the adsorbents after application compared with the adsorbents before application. Moreover, the C-OR group belongs to the TC molecule. This indicated that TC was successfully adsorbed on the surface of the adsorbent (Figs. 9a and c). As shown in Figs. 9b and d, XPS characterization results showed that the binding energy of Mn did not change before and after adsorption. However, compared with the Mn species before application, the peak area of the Mn species decreased, indicating that TC was adsorbed onto the MnO_2. In other words, a large number of TC molecules were adsorbed by MnO_2 nanoparticles loaded on both sides of TEG and covered on their surface, which made the characteristic peak area of Mn species in XPS spectra become weaker. As shown in Table 2, the pseudo-second-order kinetic model could better describe the adsorption process and proved that the adsorption process was selective chemisorption. Therefore, the above results had proved that MnO_2 nanoparticles on TEG surface could form a coordination bond with N on the dimethylamine in TC molecules, so as to achieve the purpose of TC adsorption.

In summary, the introduction of MnO_2 nanoparticles greatly enhanced the adsorption performance of TC on the 60%MnO_2/TEG (Table 5). In other words, loading MnO_2 nanoparticles on the surface of TEG to form a composite material not only increases the interaction between the composite and TC molecules and improves the TC adsorption rate, but also enables the material to better remove TC residues in pharmaceutical wastewater.

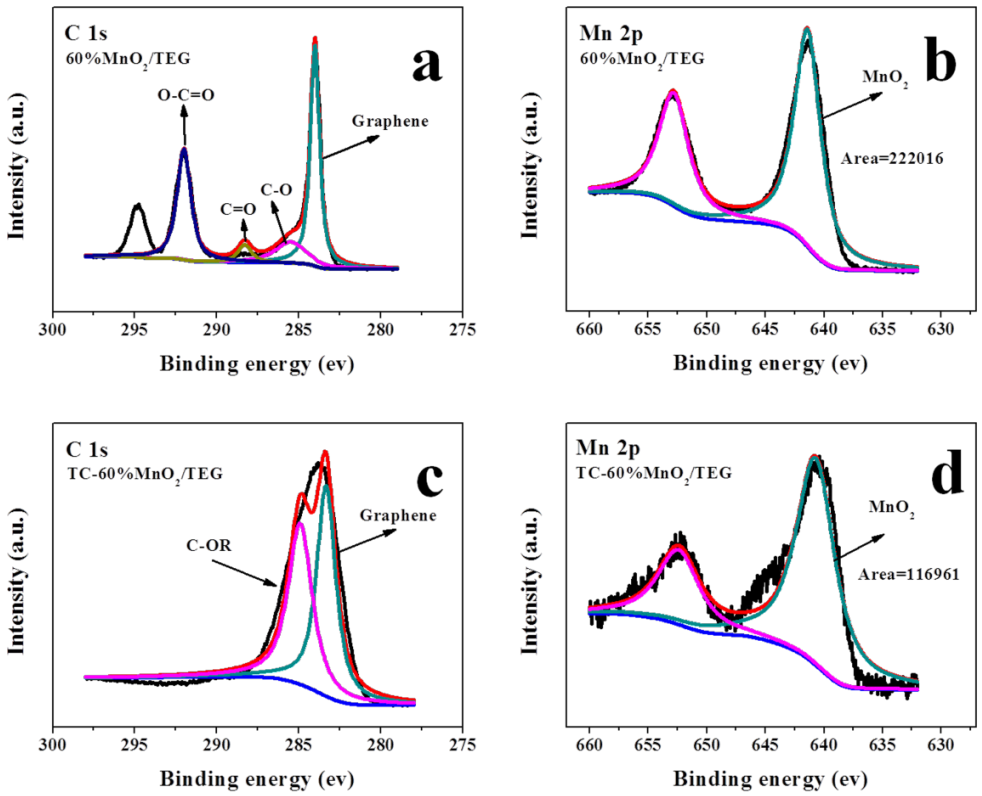

Fig. 9 . XPS patterns of (a) ~ (b) 60%MnO_2/TEG and (c) ~ (d) TC-60%MnO_2/TEG.

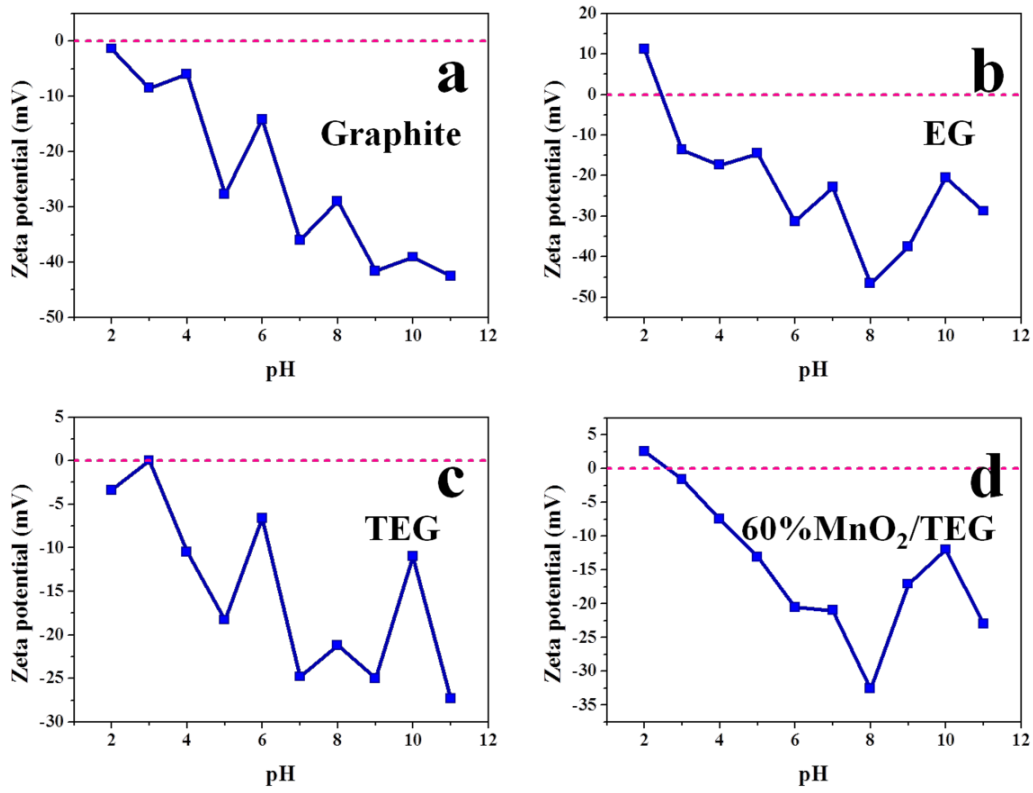

Fig. 10. Zeta potential of adsorbents at different pH values.

4. Conclusion

Here, MnO_2/TEG composites were successfully synthesized in this study. The composite material not only can exert the advantages of the carrier in the material, but also exert enhanced adsorption function from the material supported on carrier. In order to reduce the pressure of the adsorption process, the pharmaceutical wastewater needs to be flocculated to remove impurities before the adsorption test. In the whole adsorption process, the adsorption data could be well described by pseudo-second-order kinetic and Langmuir equation. The MnO_2 nanoparticles were supported on the surface of TEG to form a composite material with high selective adsorption to TC (99.2%), which could solve the problem of urgent demand for high-efficiency and low-cost adsorbents by local pharmaceutical companies.

Acknowledgements

The authors would like to thank the National Natural Science Foundation of China (No. 21467023), the National First-rate Discipline Construction Project of Ningxia (NXYLXK2017A04), and the Science and Technology Support Program of Ningxia for financial support.

References

[1] J. Wang, R. Liu, X. Yin, Adsorptive removal of tetracycline on graphene oxide loaded with titanium dioxide composites and photocatalytic regeneration of the adsorbents, J. Chem. Eng. Data, 63 (2018) 409–416.
[2] C. Wang, G. Qu, T. Wang, F. Deng, D. Liang, Removal of tetracycline antibiotics from wastewater by pulsed corona discharge plasma coupled with natural soil particles, Chem. Eng. J., 346 (2018) 159–170.
[3] J. Park, A. Nam, J. Kim, S. Yun, J. Choi, S. Lee, Blend-electrospun graphene oxide/Poly(vinylidene fluoride) nanofibrous membranes with high flux, tetracycline removal and antifouling properties, Chemosphere, 207 (2018) 347–356.
[4] X. Wang, Z. Chen, J. Kang, X. Zhao, J. Shen, Removal of tetracycline by aerobic granular sludge and its bacterial community dynamics in SBR, RSC Adv., 8 (2018) 18284–18293.
[5] L. Wang, W. Ben, Y. Li, C. Liu, Z. Qiang, Behavior of tetracycline and macrolide antibiotics in activated sludge process and their subsequent removal during sludge reduction by ozone, Chemosphere, 206 (2018) 184–191.
[6] H. Dong, Z. Jiang, C. Zhang, J. Deng, K. Hou, Y. Cheng, L. Zhang, G. Zeng, Removal of tetracycline by Fe/Ni bimetallic nanoparticles in aqueous solution, J. Colloid Interf. Sci., 513 (2018) 117–125.
[7] W. Xiong, G. Zeng, Z. Yang, Y. Zhou, C. Zhang, M. Cheng, Y. Liu, L. Hu, J. Wan, C. Zhou, R. Xu, X. Li, Adsorption of tetracycline antibiotics from aqueous solutions on nanocomposite multi-walled carbon nanotube functionalized MIL-53(Fe) as new adsorbent, Sci. Total Environ., 627 (2018) 235–244.
[8] Z. Zhang, H. Li, H. Liu, Insight into the adsorption of tetracycline onto amino and amino-Fe^{3+}functionalized mesoporous silica: Effect of functionalized groups, J. Environ. Sci.-China, 65 (2018) 171–178.
[9] X. Jiang, Y. Guo, L. Zhang, W. Jiang, R. Xie, Catalytic degradation of tetracycline hydrochloride by persulfate activated with nano Fe0 immobilized mesoporous carbon, Chem. Eng. J., 341 (2018) 392–401.
[10] G. Moussavi, A. Mashayekh-Salehi, K. Yaghmaeian, A. Mohseni-Bandpei, The catalytic destruction of antibiotic tetracycline by sulfur-doped manganese oxide (S-MgO) nanoparticles, J. Environ. Manage., 210 (2018) 131–138.
[11] J. Liu, S. Zhong, Y. Song, B. Wang, F. Zhang, Degradation of tetracycline hydrochloride by electro-activated persulfate oxidation, J. Electroanal. Chem., 809 (2018) 74–79.
[12] J. Cao, Z. Xiong, B. Lai, Effect of initial pH on the tetracycline (TC) removal by zero-valent iron adsorption, oxidation and reduction, Chem. Eng. J., 343 (2018) 492–499.
[13] S. Liang, H. Lin, X. Yan, Q. Huang, Electro-oxidation of tetracycline by a magnéli phase Ti_4O_7 porous anode kinetics, products, and toxicity, Chem. Eng. J., 332 (2018) 628–636.
[14] S.H. Yun, E.H. Jho, S. Jeong, S. Choi, Y. Kal, S. Cha, Photodegradation of tetracycline and sulfathiazole individually and in mixtures, Food Chem. Toxicol., 116 (2018) 108–113.
[15] D. Wang, F. Jia, H. Wang, F. Chen, Y. Fang, W. Dong, G. Zeng, X. Li, Q. Yang, X. Yuan, Simultaneously efficient adsorption and photocatalytic degradation of tetracycline by Fe-based MOFs, J. Colloid Interf. Sci., 519 (2018) 273–284.
[16] F. Guo, W. Shi, H. Wang, M. Han, W. Guan, H. Huang, Y. Liu, Z. Kang, Study on highly enhanced photocatalytic tetracycline degradation of typeII AgI/$CuBi_2O_4$ and Z-scheme AgBr/$CuBi_2O_4$ heterojunction photocatalysts, J. Hazard. Mater., 349 (2018) 111–118.
[17] Q. Yan, C. Li, C. Lin, Y. Zhao, M. Zhang, Visible light response AgBr/Ag_3PO_4 hybrid for removal of anionic dye and tetracycline hydrochloride in water, J. Mater. Sci-Mater. El., 29 (2018) 2517–2524.
[18] Y. Zhou, Q. Yang, D. Zhang, N. Gan, Q. Li, J. Cuan, Detection and removal of antibiotic tetracycline in water with a highly stable luminescent MOF, Sensor. Actuat. B-Chem., 262 (2018) 137–143.
[19] H. Alidadi, M. Dolatabadi, M. Davoudi, F. Barjasteh-Askaric, F. Jamali-Behnam, A. Hosseinzadeh, Enhanced removal of tetracycline using modified sawdust optimization, isotherm, kinetics, and regeneration studie, Process Saf. Environ., 117 (2018) 51–60.
[20] Z. Song, Y.L. Ma, C.E. Li, M. Xu, Removal of tetracycline residue from pharmaceutical wastewater by using 3D composite film, Chem. Eng. J., 348 (2018) 898–907.
[21] S. Nasseri, S. Ebrahimi, M. Abtahi, R. Saeedi, Synthesis and characterization of polysulfone/graphene oxide nano-composite membranes for removal of bisphenol A from water, J. Environ. Manage., 205 (2018) 174–182.
[22] H.M. Jang, S. Yoo, Y. Choi, S. Park, E. Kan, Adsorption isotherm, kinetic modeling and mechanism of tetracycline on Pinus taeda-derived activated biochar, Bioresour. Technol., 259 (2018) 24–31.
[23] M. Li, Y. Liu, S. Liu, G. Zeng, X. Hu, X. Tan, L. Jiang, N. Liu, J. Wen, X. Liu, Performance of magnetic graphene oxide diethylenetriaminepentaacetic acid nanocomposite for the tetracycline and ciprofloxacin adsorption in single and binary systems, J. Colloid Interf. Sci., 521 (2018) 150–159.
[24] T. Selmi, A. Sanchez-Sanchez, P. Gadonneix, J. Jagiello, M. Seffen, H. Sammouda, A. Celzard, V. Fierro, Tetracycline removal with activated carbons produced by hydrothermal carbonisation of Agave americanafibres and mimosa tannin, Ind. Crop. Prod., 115 (2018) 146–157.
[25] Q. Qin, X. Wu, L. Chen, Z. Jiang, Y. Xu, Simultaneous removal of tetracycline and Cu(II) by adsorption and coadsorption using oxidized activated carbon, RSC Adv., 8 (2018) 1744–1752.
[26] S. Ardashiri, S. Hashemi, B. Ramavandi, S. Dobaradaran, Modifying Amygdalus scoparia biochar with MgO for eliminating tetracycline from aqueous solutions, Desal. Water Treat., 111 (2018) 351–360.
[27] M.R. Azhar, H.R. Abid, V. Periasamy, H. Sun, M.O. Tade, S. Wang, Adsorptive removal of antibiotic sulfonamide by UiO-66 and ZIF-67 for wastewater treatment, J. Colloid Interf. Sci., 500 (2017) 88–95.
[28] Y. Guo, W. Huang, B. Chen, Y. Zhao, D. Liu, Y. Sun, B. Gong, Removal of tetracycline from aqueous solution by MCM-41-zeolite A loaded nano zero valent iron: Synthesis, characteristic, adsorption performance and mechanism, J. Hazard. Mater., 339 (2017) 22–32.
[29] T. Wang, X. Pan, W. Ben, J. Wang, P. Hou, Z. Qiang, Adsorptive removal of antibiotics from water using magnetic ion exchange resin, J. Environ. Sci.-China, 52 (2016) 111–117.

[30] M. Li, Y. Liu, G. Zeng, S. Liu, X. Hu, D. Shu, L. Jiang, X. Tan, X. Cai, Z. Yan, Tetracycline absorbed onto nitrilotriacetic acid-functionalized magnetic graphene oxide: Influencing factors and uptake mechanism, J. Colloid Interf. Sci., 485 (2017) 269–279.
[31] J. Jaafari, M.G. Ghozikali, A. Azari, M.B. Delkhosh, A.B. Javid, A.A. Mohammadi, S. Agarwal, V.K. Gupta, M. Sillanpää, A.G. Tkachev, Adsorption of p-Cresol on Al_2O_3 coated multi-walled carbon nanotubes: Response surface methodology and isotherm study, J. Ind. Eng. Chem., 57 (2018) 396–404.
[32] M. Ahmadi, H.R. Motlagh, N. Jaafarzadeh, A. Mostoufi, R. Saeedi, G. Barzegar, S. Jorfi, Enhanced photocatalytic degradation of tetracycline and real pharmaceutical wastewater using MWCNT/TiO_2 nano-composite, J. Environ. Manage., 186 (2017) 55–63.
[33] S. Agarwal, I. Tyagi, V.K. Gupta, M. Dehghani, J. Jaafari, D. Balarak, M. Asif, Rapid removal of noxious nickel (II) using novel γ-alumina nanoparticles and multiwalled carbon nanotubes: Kinetic and isotherm studies, J. Mol. Liq., 224 (2016) 618–623.
[34] Z. Song, Y.L. Ma, C.E. Li, The residual tetracycline in pharmaceutical wastewater was effectively removed by using MnO_2/graphene nanocomposite, Sci. Total Environ., 651 (2019) 580–590.
[35] R. Zandipak, S. Sobhanardakani, Novel mesoporous Fe_3O_4/SiO_2/CTAB-SiO_2 as an effective adsorbent for the removal of amoxicillin and tetracycline from water, Clean Technol. Environ., 20 (2018) 871–885.
[36] Y. Zhang, Z. Jiao, Y. Hu, S. Lv, H. Fan, Y. Zeng, J. Hu, M. Wang, Removal of tetracycline and oxytetracycline from water by magnetic Fe_3O_4@graphene, Environ. Sci. Pollut. R., 24 (2017) 2987–2995.
[37] C. Xu, C. Jiao, R. Yao, A. Lin, W. Jiao, Adsorption and regeneration of expanded graphite modified by CTAB-KBr/H_3PO_4 for marine oil pollution, Environ. Pollut., 233 (2018) 194–200.
[38] C. Xu, H. Wang, W. Yang, L. Ma, A. Lin, Expanded graphite modified by CTAB-KBr/H_3PO_4 for highly efficient adsorption of dyes, J. Polym. Environ., 26 (2018) 1206–1217.
[39] J.M. Lv, Y.L. Ma, X. Chang, S.B. Fan, Removal and removing mechanism of tetracycline residue from aqueous solution by using Cu-13X, Chem. Eng. J., 273 (2015) 247–253.
[40] M. Abtahi, A. Mesdaghinia, R. Saeedi, S. Nazmara, Biosorption of As (III) and As (V) from aqueous solutions by brown macroalga Colpomeniasinuosa biomass: kinetic and equilibrium studies, Desal. Water Treat., 51 (2013) 3224–3232.
[41] K. Naddafi, N. Rastkari, R. Nabizadeh, R. Saeedi, M. Gholami, M. Sarkhosh, Adsorption of 2, 4, 6-trichlorophenol from aqueous solutions by a surfactant-modified zeolitic tuff: batch and continuous studies, Desal. Water Treat., 57 (2016) 5789–5799.
[42] K. Naddafi, R. Saeedi, Biosorption of copper (II) from aqueous solutions by brown macroalga Cystoseiramyrica biomass, Environ. Eng. Sci., 26 (2009) 1009–1015.
[43] Y. Yang, X. Hu, Y. Zhao, L. Cui, Z. Huang, J. Long, J. Xu, J. Deng, C. Wu, W. Liao, Decontamination of tetracycline by thiourea-dioxide-reduced magnetic graphene oxide: Effects of pH, ionic strength, and humic acid concentration, J. Colloid Interf. Sci., 495 (2017) 68–77.